



## Characterization and application of C-TiO<sub>2</sub> doped cellulose acetate nanocomposite film for removal of Reactive Red-195

Xuan Nui Pham, Duc Trong Pham, Ha Son Ngo, Manh B. Nguyen & Huan V. Doan

To cite this article: Xuan Nui Pham, Duc Trong Pham, Ha Son Ngo, Manh B. Nguyen & Huan V. Doan (2020): Characterization and application of C-TiO<sub>2</sub> doped cellulose acetate nanocomposite film for removal of Reactive Red-195, Chemical Engineering Communications, DOI: [10.1080/00986445.2020.1712375](https://doi.org/10.1080/00986445.2020.1712375)

To link to this article: <https://doi.org/10.1080/00986445.2020.1712375>



Published online: 13 Jan 2020.



Submit your article to this journal [↗](#)




View related articles [↗](#)



View Crossmark data [↗](#)



## Characterization and application of C-TiO<sub>2</sub> doped cellulose acetate nanocomposite film for removal of Reactive Red-195

Xuan Nui Pham<sup>a</sup>, Duc Trong Pham<sup>a</sup>, Ha Son Ngo<sup>a</sup>, Manh B. Nguyen<sup>b</sup>, and Huan V. Doan<sup>a,c</sup> 

<sup>a</sup>Department of Chemical Engineering, Hanoi University of Mining and Geology, Hanoi, Vietnam; <sup>b</sup>Institute of Research and Development, Duy Tan University, Da Nang, Vietnam; <sup>c</sup>Department of Mechanical Engineering, University of Bristol, Bristol, UK

### ABSTRACT

This article introduces research on the synthesis and characteristics of C-TiO<sub>2</sub> doped cellulose acetate (CA) nanocomposite film. TiO<sub>2</sub> nanoparticles were synthesized from Ilmenite mineral in Binh Dinh, Vietnam, and modified by *Stevia Rebaudiana* plant in order to serve as a cheap, stable, and eco-friendly photocatalyst that could perform under visible light. Nanocomposite film was obtained by dispersing C-TiO<sub>2</sub> on cellulose acetate polymer using a supersonic generator. The prepared material was characterized by X-ray diffractions (XRD), N<sub>2</sub> adsorption, Raman spectroscopy, Fourier-transform infrared spectroscopy (FT-IR), energy-dispersive X-ray analysis (EDX), UV-Vis diffuse reflectance spectroscopy (UV-vis DRS), photoluminescence (PL) emission spectra, scanning electron spectroscopy (SEM), and thermogravimetric/differential thermal analysis (TG-DTA). The film's photocatalytic efficiency was evaluated via the decomposition of Reactive Red-195 (RR-195) under visible irradiation at room temperature. The results showed that the maximum conversion of RR-195 reached 99.15% at pH = 3 and the activity of the catalyst had a slight decrease after up to four times of recycling, for which the conversion of the fourth reaction was 90.02% for RR-195. This result suggests an efficient treatment method to eliminate organic pollutants from wastewater and stimulate these industrial activities in Vietnam.

### KEYWORDS

Cellulose acetate; C-TiO<sub>2</sub>; degradation; film; ilmenite; photocatalyst

### Introduction

The increasing amount of waste from human activity is one of the most urgent environmental challenges to be faced at the present time (Gaya and Abdullah 2008; Ortega-Liébana et al. 2012; Pelaez et al. 2012). Among these waste products, organic compounds in wastewater, that are stable and difficult to bio-degrade, account for a significant portion, and have become a problem in pollution management as well as in water reuse. Conventional treatments such as adsorption, precipitation, etc., are not suitable for dealing with new pollutants which are more and more diversified in type and quantity. In addition, these traditional methods require high initial investment and operating costs as well as create undesired pollutants. Therefore, the appearance of alternative methods for water treatment that are efficient, economic, and eco-friendly seems to be

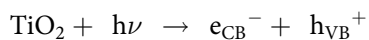
natural, and advanced oxidation processes (AOPs) (Barndök et al. 2013; Gaya and Abdullah 2008; Ibhaddon and Fitzpatrick 2013) using photocatalysts are typical examples. In AOPs, the presence of photocatalysts, radicals, and intermediates (H<sub>2</sub>O<sub>2</sub>, <sup>•</sup>OH, <sup>•</sup>O<sub>2</sub><sup>-</sup>, O<sub>3</sub>) plays the role of oxidation agents that could completely oxidize and mineralize pollutants. By employing a photocatalyst, these processes could be carried out in mild conditions with energy from sunlight that minimizes operational costs (Barndök et al. 2013; Ortega-Liébana et al. 2012). TiO<sub>2</sub>, the most popular semiconductor, is widely used as a photocatalyst in the various processes including AOPs because TiO<sub>2</sub> appears to be more stable and easier to synthesize than others (Kubacka et al. 2012; Ortega-Liébana et al. 2012; Pelaez et al. 2012). The oxidation process mechanism catalyzed by TiO<sub>2</sub> could be as suggested below:

**CONTACT** Xuan Nui Pham  phamxuannui@humg.edu.vn; phamxuannui@gmail.com 

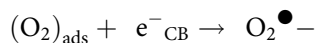
Color versions of one or more of the figures in the article can be found online at [www.tandfonline.com/gcec](http://www.tandfonline.com/gcec).

© 2020 Taylor & Francis Group, LLC

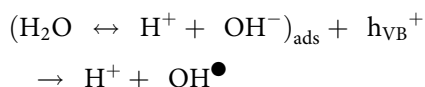
- Photo absorption of  $\text{TiO}_2$  ( $h\nu \geq E_g = 3.2 \text{ eV}$ )



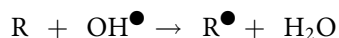
- Reaction of  $\text{O}_2$  with electron



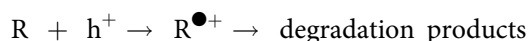
- Reaction of hole



- Oxidation by hydroxyl radical



- Or by hole



However,  $\text{TiO}_2$  has a large band gap energy that requires ultraviolet irradiation. Thus, narrowing the energy gap of  $\text{TiO}_2$  to improve visible light absorption is one of the common methods used to boost photocatalytic performance (Kubacka et al. 2012). The methods commonly used are the addition of metals or metal oxides, into the  $\text{TiO}_2$  lattice, such as Zn, Fe, Cr, Eu, Y, Ag, Ni, etc. or adding N, C, S, F, Cl, etc. or putting a mixture of elements into the  $\text{TiO}_2$  lattice (Papadam et al. 2007). Among them,  $\text{TiO}_2$  modified by carbon is particularly interesting because several studies have shown that: in the process of modification, carbon has doped into the  $\text{TiO}_2$ , narrowing the initial bandgap of  $\text{TiO}_2$ . Different evaluations of photocatalytic ability under visible light demonstrated the superior photocatalytic ability of C- $\text{TiO}_2$  materials compared to unmodified materials. Momeni et al. (2016a, 2016b) reported fabrication of nitrogen, carbon, and iron multiple-codoped titanium dioxide nanotubes by depositing method on  $\text{TiO}_2$  nanotube surface as a new high-performance photocatalyst. At the same time, these authors also synthesized the photocatalytic nanocomposite films of  $\text{Ag}_2\text{S}/\text{TiO}_2$  by electrochemical anodizing and successive ionic layer adsorption and reaction approach (Momeni et al. 2016a, 2016b). Iron-cobalt  $\text{WTiO}_2$  nanotube (WTNTs) films prepared by the chemical bath deposition method (Momeni et al. 2019). However, these catalysts have several drawbacks, such as the intricacy in recovering from solution for reuse and the tendency to accumulate and harm living organisms when exposed to the

environment (Wang et al. 2015). Therefore, to deal with these issues, the carbon source for the modification in our study comes from plant sources, so it is very environmentally friendly and simple to synthesize.

Since the 1960s, polymer membrane technologies have become dominant for water treatment with very competitive cost (Liu et al. 2011). Among them, cellulose acetate film is considered an typical membrane as it has moderate flux and high salt characteristics as well as its bountiful raw sources (Radha et al., 2014). In addition, organic polymer membranes are biodegradable. Nevertheless, the polymer membrane is susceptible to fouling due to the accumulation of contaminants and bacteria on the surface or inside of the membrane, which limits the wide application of membranes, since this accumulation can cause many adverse effects such as poor water quality, low water treatment productivity, high energy use, and shorter membrane life (Bai et al. 2010; Kang and Cao 2014; Radha et al. 2014). To solve this problem, two methods utilizing  $\text{TiO}_2$  nanomaterials have been studied by scientists: (1) changing the surface properties of the membrane by using objects nano- $\text{TiO}_2$  inorganic materials (Liu et al. 2011; Meng et al. 2009; Wang et al. 1997), and (2) the combination of adsorption functions, photosynthesis of organic substances of  $\text{TiO}_2$  to control and limit accumulation (Zhang et al. 2014). Remarkably, the nanostructures of  $\text{TiO}_2$  create many active centers for photocatalytic reaction and adsorption of pollutants. Several studies involving cellulose acetate polymer films in combination with  $\text{TiO}_2$  have been published. Typically, Wang et al. synthesized cellulose acetate @ $\text{TiO}_2$  fiber by an electrospinning method of methylene blue decomposition, the highest conversion rate reached 90% after 240 min but this process requires UV irradiation to consume energy (Wang et al. 2015), and Abedini et al. dispersed  $\text{TiO}_2$  nanoparticles on cellulose acetate membranes by phase reversal and studied the permeability properties of membranes. The  $\text{TiO}_2$  used in the Abedini study was from a source of toxic and expensive organic titanium (Abedini et al. 2011). Jinlong et al. (2018) synthesized a new three-dimensional, flower-like La- $\text{TiO}_2/\text{g-C}_3\text{N}_4$  heterojunction composite as photocatalyst using a solvothermal method. A novel Gd/ $\text{TiO}_2$ @rGO nanocomposite with high photocatalytic

performance were prepared by *via* a one-pot solvothermal method (Shuaiqiang et al. 2019).

In this study, novel biodegradable C-TiO<sub>2</sub>/CA photocatalytic nanocomposite film was prepared by the phase inversion method using natural material sources from Vietnam. To do that, TiO<sub>2</sub> were synthesized using Ilmenite mineral collected directly in Binh Dinh, Vietnam. These TiO<sub>2</sub> materials were then denatured into C-TiO<sub>2</sub> with carbon derived from *Stevia* leaves and dispersed on cellulose acetate polymer films in order to serve as a cheap, stable, and eco-friendly photocatalyst that could work under visible irradiation. After that, the photocatalytic efficiency of the material at different pH was investigated in the decomposition of RR-195 (Reactive Red-195) under visible irradiation and ambient temperature.

## Experimentals

### Chemicals

Ilmenite mineral came from Binh Dinh, Vietnam. The stevia leaves (*Stevia rebaudiana*) were purchased from Vietnam. Cellulose acetate (AC, MW = 25,000 Da) was purchased from Sigma-Aldrich; hydrofluoric acid (40 wt.% HF), potassium chloride (KCl), and ammonia (28 wt.% NH<sub>3</sub> in water) purchased from China; N,N'-dimethylformamide, Reactive Red-195 (RR-195, 99%) was acquired from Aldrich. The chemicals were utilized without any purification.

### Recovery of titanium dioxide (TiO<sub>2</sub>) from ilmenite mineral

Ilmenite was resolved by 8.4 M HF solution, stirred for 5 h at a speed of 300 rpm, then deposited and filtered to remove residue. The filtered water was collected.

Saturated KCl solution was gradually put in to the stirring filtrate solution, Ti<sup>4+</sup> ions were separated from iron in the form of precipitated K<sub>2</sub>TiF<sub>6</sub> salt. Then, distilled water was used to wash the precipitate to neutral pH to eliminate impurities and then the solid was dried.

Next, the obtained K<sub>2</sub>TiF<sub>6</sub> was dissolved in hot water at 80 °C to saturated concentration (60.224 g/l). Then, 4 M NH<sub>3</sub> solution was slowly added to obtain a mixture with pH = 9–10. At the end of hydrolysis,

the Ti(OH)<sub>4</sub> product was collected by filtration, washed with distilled water, dried at 105 °C for 2 h then calcined at 450 °C for 3 h.

### Synthesis of carbon doped-nano TiO<sub>2</sub> (C-TiO<sub>2</sub>)

The stevia leaves were dried at 100 °C before grinding into a fine powder. Then 2.5 g of the powder was pyrolyzed in the furnace for 2 h at 300 °C. The obtained black carbon powder was cooled down to room temperature, then added in distilled water, and centrifuged at 2500 rpm to remove large or agglomerated particles. After removing the solid portion, a yellow-brown solution was obtained. After that, a mixture was formed by dispersing 1 g of TiO<sub>2</sub> powder was dispersed in 5.2 mL previous solution. Next, 4.8 mL of distilled water was added and agitated strongly for 30 min. The final mixture was then desiccated at 65 °C to obtain C-TiO<sub>2</sub>.

### Synthesis of C-TiO<sub>2</sub>/AC nanocomposite films by phase inversion method

Mixtures of AC (12 wt.%) and N,N'-dimethylformamide were stirred for 5 h. C-TiO<sub>2</sub> (20 wt.% compared to AC) was added and stirred for 3 h, then used ultrasonic for 1 h. Next, the mixture was spread on a glass plate and subsequently submerged in a bath of distilled water to entirely separate the phases. The film was detached from the board glass surface, rinsed with distilled water and ethanol, and soaked in water for 12 h. A film that did not contain C-TiO<sub>2</sub> was made similarly for comparison.

### Evaluation of catalytic activity

The photocatalytic efficiency of the C-TiO<sub>2</sub>/CA film was evaluated in the degradation reaction of RR-195, a typical dye widely present in textile, paper, and printing industries. In which, a link -N=N- (azo), sulfone, and monochlorotriazine are main functional groups.

First, model wastewater was prepared by taking 20 mg RR-195 phase in 1000 mL water solvent (20 ppm).

Photocatalytic test of C-TiO<sub>2</sub>/AC film: 50 mL of RR-195 (20 ppm) solution was put into a flask,

stirred gently for 30 min in the dark then the mixture was irradiated by a 125 W high pressure Hg lamp. Then, the solution was analyzed by UV-Vis spectrometer at  $\lambda_{\max} = 541$  nm.

The conversion of RR-195 was calculated based on its initial concentration,  $C_0$  ( $\text{mg L}^{-1}$ ), and the concentration  $C_t$  ( $\text{mg L}^{-1}$ ) of RR-195 in the solution at reaction time  $t$  (min)

$$A = \left( (C_0 - C_t) / C_0 \right) \times 100\% \quad (1)$$

where  $A$  is the conversion (%) of RR-195.

In this study, the effects of catalyst weight, pH and catalytic form on the conversion of RR-195 and the ability of catalytic regeneration after use were also assessed.

### Characterizations

The crystalline phase structure of as-prepared materials was determined by XRD with the 2-theta range of  $2^\circ$ – $80^\circ$  and  $20^\circ$ – $80^\circ$  (D8 ADVANCE, Bruker, Germany) using Cu  $\text{K}\alpha_1$  copper radiation ( $k = 0.154$  nm) as the X-ray source at a scan rate of  $3 \text{ min}^{-1}$ . Nitrogen adsorption-desorption isotherms were analyzed on Automated Sorptometer BET 201-A, USA. The material morphology was studied by SEM using an S-4800 microscope (Hitachi, Japan) with an accelerating voltage of 200 kV. A JED-2300 with gold coating provided data of energy-dispersive X-ray spectroscopy analysis (EDX). In addition, UV-Vis diffuse reflection spectroscopy (DRS) was recorded on Cary 5000 within the

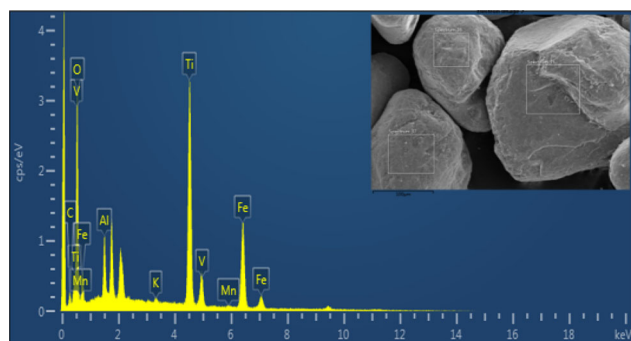


Figure 1. EDX spectra of ilmenite.

Table 1. EDX element analysis of ilmenite.

Element	Ti	O	Si	Fe	K	V	Al	Mn	C
Mass composition (%)	25.46	40.47	2.8	23.51	0.29	0.65	2.51	0.29	4.01
Atomic composition (%)	13.18	62.70	2.47	10.44	0.19	0.31	2.31	0.13	8.27

wavelength range of 200–800 nm. The photoluminescence emission spectra excited at 300 nm were recorded by a PL 3-22 JobinY von-Spex, USA spectrofluorometer Fluorolog using a 450 W xenon lamp. FT-IR spectra were obtained with FTIR Affinity – 1 s (Shimadzu) from 400 to  $4000 \text{ cm}^{-1}$  at a resolution of  $4 \text{ cm}^{-1}$ . Thermogravimetry analysis (TGA) was implemented between room temperature and  $800^\circ\text{C}$  at a rate of  $10^\circ\text{C}/\text{min}$  on a DTG-60H thermogravimetric analyzer in an air flow of  $50 \text{ mL}/\text{min}$ .

## Results and discussion

### Characterization of the materials

The composition of Binh Dinh ilmenite was determined by the EDX method, the results are presented in Figure 1 and Table 1. From the EDX results, it could be found that the mineral had quite high Ti and O content. In addition, it also contains a large amount of Fe (23.51 wt%), titanium, and iron in the composition that could facilitate the decomposition of the mineral by HF acid due to the ability to form complexes of these ions with anionic fluoride in an acidic environment. However, the high content of iron impurities in the mineral greatly affects the preparation of high purity  $\text{TiO}_2$ .

Figure 2 illustrates the XRD spectra of material samples. From Figure 2, the recorded peaks represent for anatase  $\text{TiO}_2$  (JCPDS file No. 21-1272) and no other peaks of impurities appears. The  $\text{TiO}_2$  average particle size was 20 nm determined by using the Scherrer equation:  $D = 0.9\lambda / (\beta \cos\theta)$  (where  $D$  – the mean size of the crystalline;  $\lambda$  – the X-ray wavelength;  $\beta$  is the line broadening at half the maximum intensity;  $\theta$  is the Bragg angle). After that, with the doping of carbon, the structure of C- $\text{TiO}_2$  material was unchanged, and only the  $\text{TiO}_2$  anatase phase peaks still existed (JCPDS file No. 21-1272). Figure 2 shows peaks at  $2\theta$  of  $6.26^\circ$ ,  $7.46^\circ$ ,  $8.45^\circ$  corresponding to the cellulose triacetate structure (Kono et al. 1999). In addition, when dispersing C- $\text{TiO}_2$  on CA film,

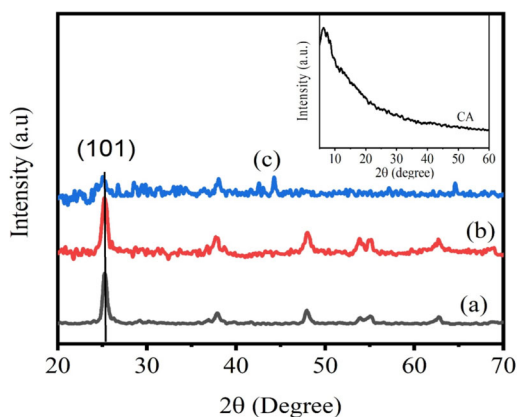


**Figure 2.** XRD spectra of the materials  $\text{TiO}_2$  (a),  $\text{C-TiO}_2$  (b),  $\text{C-TiO}_2/\text{CA}$  film (c).

peaks were still recorded at about  $2\theta = 25^\circ$ , which characterizes the anatase phase of  $\text{TiO}_2$ . Based on these results, it could be affirmed that the addition of doping carbon onto  $\text{TiO}_2$  then the dispersion of  $\text{C-TiO}_2$  on the CA film did not change the phase structure of the original  $\text{TiO}_2$  material.

The  $\text{N}_2$  adsorption-desorption isotherm of CA and  $\text{C-TiO}_2/\text{CA}$  film is shown in Figure 3. As shown in Figure 3, the samples are of type IV with a steep uptake at  $P/P_0$  of above 0.9. The BET surface area of the CA film was small with a value of  $10.22 \text{ m}^2/\text{g}$  and pore volume of  $0.056 \text{ cm}^3/\text{g}$ . However, these values increased to  $13.32 \text{ m}^2/\text{g}$  and  $0.076 \text{ cm}^3/\text{g}$  after dispersing  $\text{C-TiO}_2$  on CA film. With comparing the samples of pristine CA film and  $\text{C-TiO}_2/\text{CA}$  film, it was obvious that the  $\text{C-TiO}_2/\text{CA}$  film has a larger BET surface area and pore volume than the CA film. This difference clearly indicated the dispersion of  $\text{C-TiO}_2$  nanopartilces onto cellulose acetate polymer film.

Figure 4 reveals the Raman spectrum of C-doped  $\text{TiO}_2$ . The peaks at  $146 \text{ cm}^{-1}$  (Eg),  $199 \text{ cm}^{-1}$  (Eg, weak),  $399 \text{ cm}^{-1}$  (B1g),  $516 \text{ cm}^{-1}$  (A1g), and  $640 \text{ cm}^{-1}$  (Eg) are typical for peaks of anatase phase (Su et al. 2007; Wang et al. 2008). Also, no peaks were found at  $235$  and  $612 \text{ cm}^{-1}$  that represents for  $\text{TiO}_2$  existing in the rutile phase. This means that the material exists only in the anatase phase (Wang and Hall 1984), which is in agreement with the XRD results. The decrease in the intensity of peaks in the carbon-doped sample is explained by the disruption of the symmetry of the  $\text{TiO}_2$  molecule with the

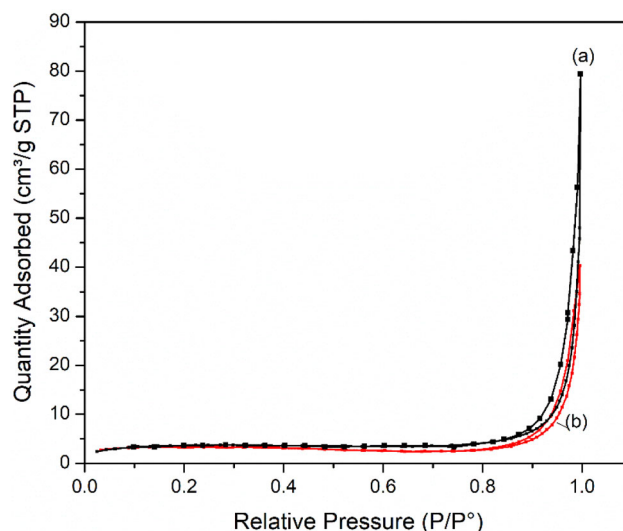


**Figure 3.**  $\text{N}_2$  adsorption-desorption isotherm of CA film (a) and  $\text{C-TiO}_2/\text{CA}$  film (b).

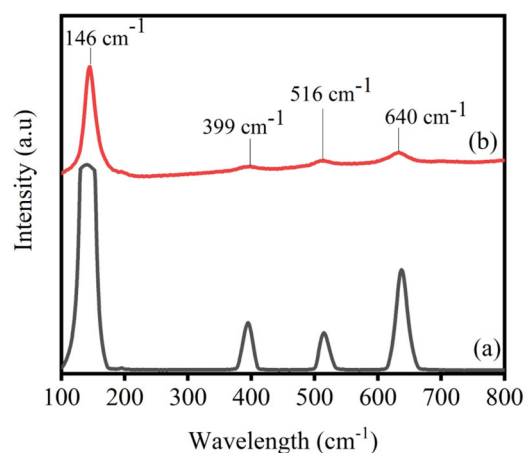


**Figure 4.** Raman spectra of  $\text{TiO}_2$  (a) and  $\text{C-TiO}_2$  (b).

presence of C in the  $\text{TiO}_2$  lattice (Wang et al. 2008). So, it can be deduced that carbon has been successfully doped into the  $\text{TiO}_2$  lattice (Bhattacharyya et al. 2008).

The bonding properties in  $\text{TiO}_2$  and C-doped  $\text{TiO}_2$  samples determined by the FT-IR spectrum are shown in Figure 5. Peaks appearing at about  $3456\text{--}3600 \text{ cm}^{-1}$  and  $1629 \text{ cm}^{-1}$  characterize the type of chemotherapy vibration of  $\nu(\text{OH})$  of surface water molecules (Ernö et al. 2009). Other peaks seen at  $1035\text{--}1187 \text{ cm}^{-1}$  of  $\text{C-TiO}_2$  are thought to be the valence oscillation type of C-O (Gong et al. 2015; Sun et al. 2015; Wang et al. 2014). The important peak at  $1658 \text{ cm}^{-1}$  could refer to the bond of C=C. The peaks in the range of  $500\text{--}800 \text{ cm}^{-1}$  represent the oscillation range of Ti-O-Ti. Indeed, surface hydroxyl groups are an

decisive factor in photocatalytic activity because the groups can react with photogenerated holes to form hydroxyl radicals that reduce the ability of electron-hole recombination, thus increasing photocatalytic efficiency (Sleiman et al. 2007). By the results of FT-IR, it is suggested that there were the surface 'OH radicals of C-TiO<sub>2</sub>. In addition, the existence of carbon could be discovered and confirmed by EDX results.

The composition of the C-TiO<sub>2</sub> sample was detected by the EDX method as presented in Figure 6 and Table 2.

From EDX results of the C-TiO<sub>2</sub> sample it was found that there was no occurrence of Fe impurities and only Ti, O, and C, which are the main components of C-TiO<sub>2</sub>, could be seen. This suggested that the mineral decomposition process had completely eliminated iron impurities although the initial iron content in the mineral

was relatively high. Moreover, there was also the presences of K and F left because of the TiO<sub>2</sub> washing process.

Photocatalytic properties of TiO<sub>2</sub> and C-TiO<sub>2</sub> materials were determined by UV-vis spectrometry. Figure 7(a) illustrates the UV-vis DRS spectrum of C-TiO<sub>2</sub> and TiO<sub>2</sub>. The band gap of the samples calculated using the transformed Kubelka-Munk function versus energy of light is shown in Figure 7(b).

As can be seen, large optical absorption C-TiO<sub>2</sub> can be observed in visible light. According to the research by Kish et al., the presence of carbon content in TiO<sub>2</sub> has a great influence on the light absorption of the material (Sakthivel and Kisch 2003). In fact, the substitution of oxygen atoms in the Titania lattice by C, N, F, P, or S could lower the TiO<sub>2</sub> band gap and result in the ability to excite the photocatalysts with both UV and visible irradiation. So, the visible light absorption ability of C-TiO<sub>2</sub> is greater than TiO<sub>2</sub> due to the addition of carbon. Based on the Kubelka-Munk method, the bandgap energy can be calculated by taking the intersection of the tangent line of the graph  $(\alpha h\nu)^{1/2}$  with the photon energy ( $h\nu$ ). The values of TiO<sub>2</sub> and C-TiO<sub>2</sub> are 3.1 eV and 2.85 eV, respectively. The optical band gap value 3.1 eV for pure TiO<sub>2</sub> corresponds to the anatase TiO<sub>2</sub> consistent with XRD data indicating the anatase phase as the major phase. The value 2.85 eV again confirms the reduction of the bandgap induced by the introduction of C into the TiO<sub>2</sub> matrix.

Moreover, if titanium ions in TiO<sub>2</sub> are replaced by carbon, visible light absorption is not

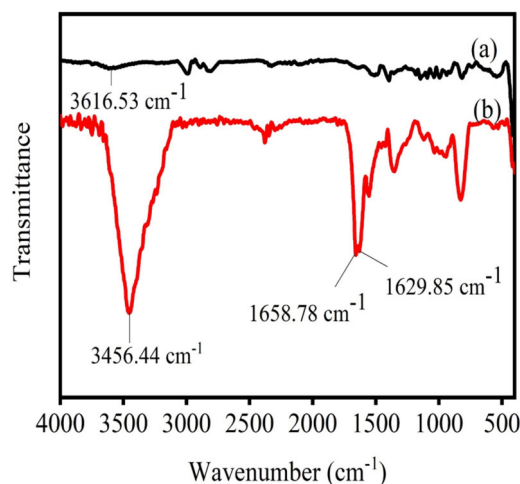


Figure 5. FT-IR spectra of TiO<sub>2</sub> (a) and C-doped TiO<sub>2</sub> (b).

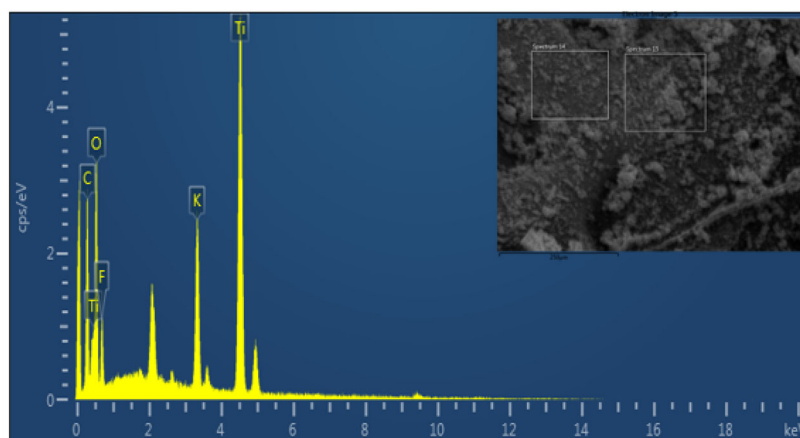


Figure 6. EDX spectrum of C doped TiO<sub>2</sub>.

observed (Kamisaka et al. 2005). Thus, it is believed that the bandgap energy of the carbon-doped  $\text{TiO}_2$  sample is significantly reduced when compared to the pure  $\text{TiO}_2$  sample due to the replacement of oxygen in  $\text{TiO}_2$  by carbon atoms, thus permitting visible light absorption.

In order to further demonstrate photocatalytic efficiency of C- $\text{TiO}_2$ /CA film, the photoluminescence emission was investigated using A 450 W xenon lamp at excitation wavelength of 300 nm. The obtained results are shown in Figure 8. Compared with  $\text{TiO}_2$ /CA photocatalyst film, after the carbon modification, the PL intensity of  $\text{TiO}_2$  nanoparticles were significantly decreased, indicating that the carbon modification lowered recombination rate of electron/hole of the photocatalyst film.

Scanning electron microscopy (SEM) method was used to study the morphology of acetate cellulose film (CA) and C- $\text{TiO}_2$ /CA film (Figure 9).

The morphological structure of cellulose acetate (CA) film is illustrated by the film surface in Figure 9(a<sub>1</sub>) and the cross-section in Figure 9(a<sub>2</sub>) which present the structural association of cellulose acetate molecules in the polymer chain in combination with pores in the material structure. The formation of pores could be explained by the fragmentation of the polymer chain (Ioniță et al. 2018). C- $\text{TiO}_2$  nanoparticles were observed on the surface of CA in Figure 9(b<sub>1</sub>). Comparing

with the morphology of the CA film in Figure 9(a<sub>1</sub>), it could be seen that the average size of C- $\text{TiO}_2$  is about 20–30 nm (in accordance with the calculation method in XRD) which has been evenly distributed on the polymer chain surface. The cross-sectional SEM image of C- $\text{TiO}_2$ /CA film revealed that the porous structure of the material remained intact after adding nano-C- $\text{TiO}_2$  into CA film. The pore structure of the material will contribute to enhancing the contact ability of C- $\text{TiO}_2$  nanoparticles with pollutants.

TGA was used to investigate the thermal properties of CA and C- $\text{TiO}_2$ /CA films and the measured data are shown in Figure 10.

According to this figure, the mass loss of samples was calculated at 99% and 84% corresponding to CA film and C- $\text{TiO}_2$ /CA film. When C- $\text{TiO}_2$  was added onto the CA film, the mass loss of the film decreased resulting in the residual

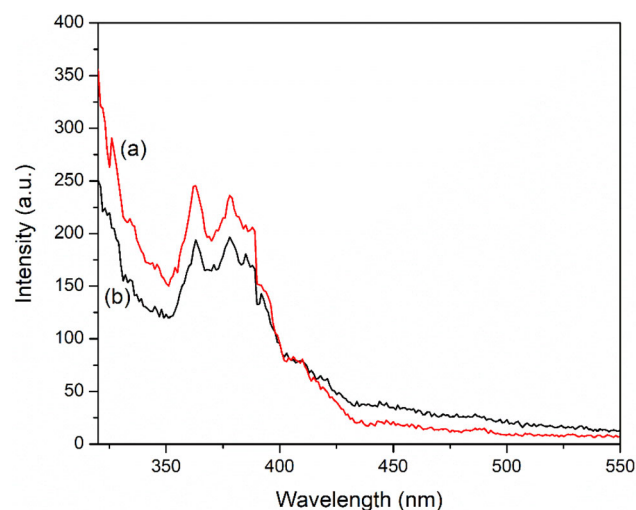


Figure 8. Photoluminescence emission spectra (excited at 300 nm) of  $\text{TiO}_2$ /CA film (a) and C- $\text{TiO}_2$ /CA film (b).

Table 2. EDX element analysis of C doped  $\text{TiO}_2$  sample.

Element	Ti	O	C	F	K
Mass composition (%)	26.87	33.57	23.81	9.4	6.34
Atomic composition (%)	10.59	39.60	37.41	9.34	3.06

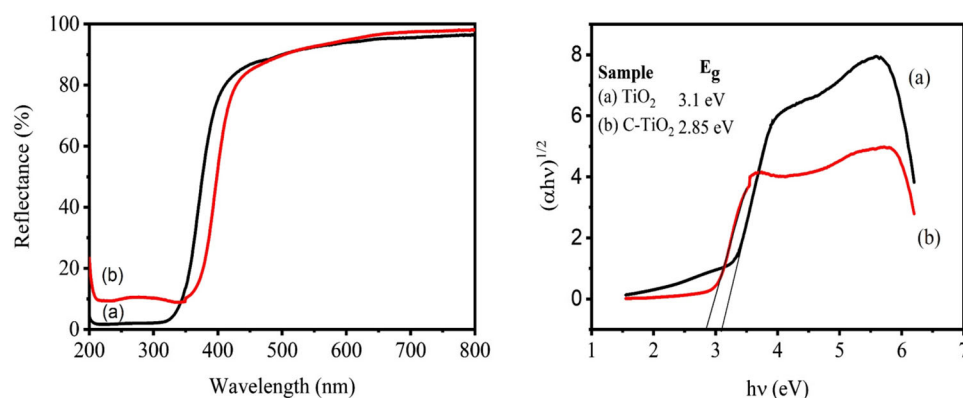
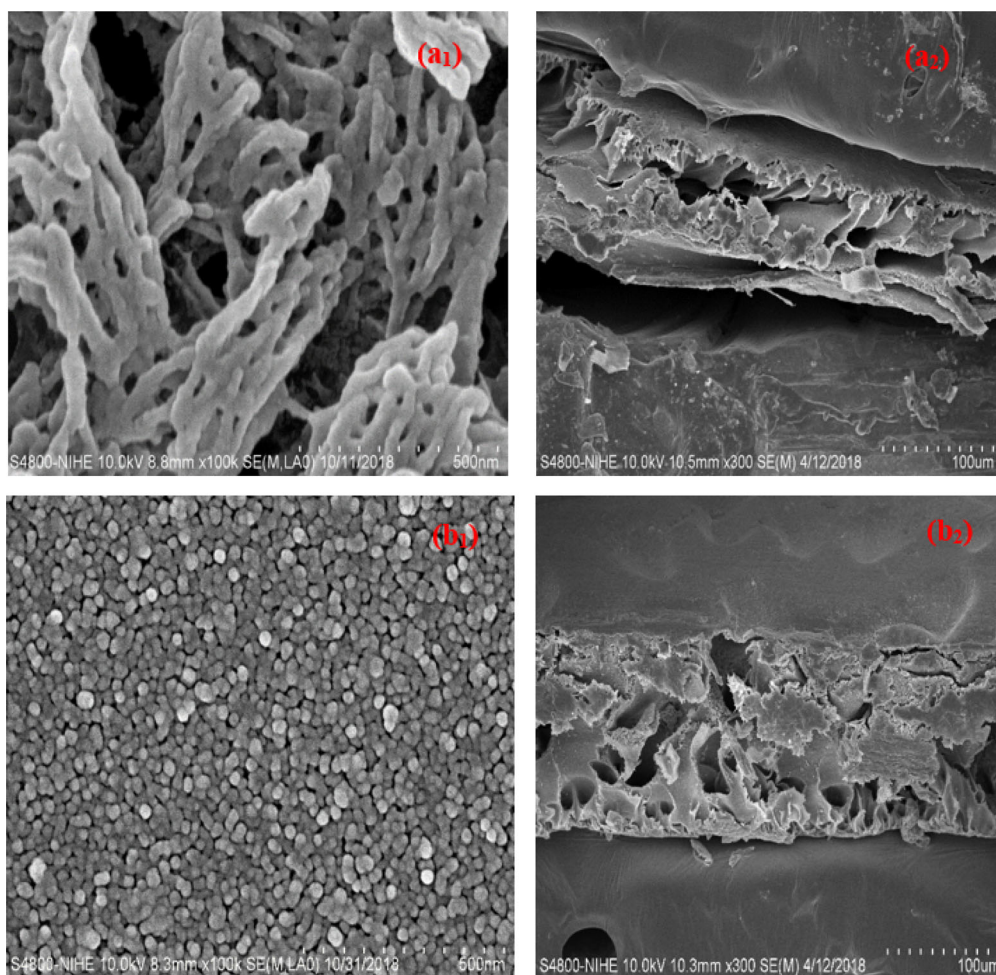
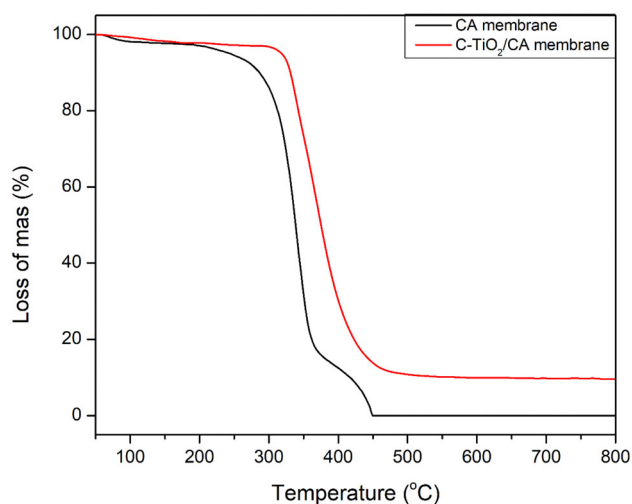


Figure 7. UV-vis DRS spectra and transformed Kubelka-Munk with the energy of the excitation source of  $\text{TiO}_2$  (a) and C-doped  $\text{TiO}_2$  (b).





**Figure 9.** SEM images of acetate cellulose (CA) film (a): film surface (a<sub>1</sub>), cross section (a<sub>2</sub>); and C-TiO<sub>2</sub>/CA nanocomposite (b): film surface (b<sub>1</sub>), cross section (b<sub>2</sub>).



**Figure 10.** Thermal gravimetric analysis (TGA) curves of (a) CA and (b) C-TiO<sub>2</sub>/CA film.

mass of the C-TiO<sub>2</sub>/CA film being higher than that of the CA film. This could originate from the removal of heat in the material. Specifically, the additional heat is transferred to C-TiO<sub>2</sub> in

the film during the analysis process. Thanks to the interaction between C-TiO<sub>2</sub> and CA based on hydrogen bonds or covalents which improve the energy of the CA chain, the strength of the polymer chain would be reinforced. Therefore, the improvement of thermal resistance could be due to a slight increase in the decomposition temperature of the C-TiO<sub>2</sub>/CA film (T<sub>d</sub>) with the presence of C-TiO<sub>2</sub>. In fact, similar results were observed by Abedini et al. (2011). According to the authors, good compatibility between CA and C-TiO<sub>2</sub> was achieved because of the bond of Ti<sup>4+</sup> and acetate groups as well as the creation of the hydrogen link between surface OH groups and acetate groups of CA (Abedini et al. 2011). Moreover, the significant interaction between C-TiO<sub>2</sub> and the CA chain can prevent C-TiO<sub>2</sub> from being easily separated from the film. An increase of about 15% was recorded in the thermal resistance of the C-TiO<sub>2</sub> sample

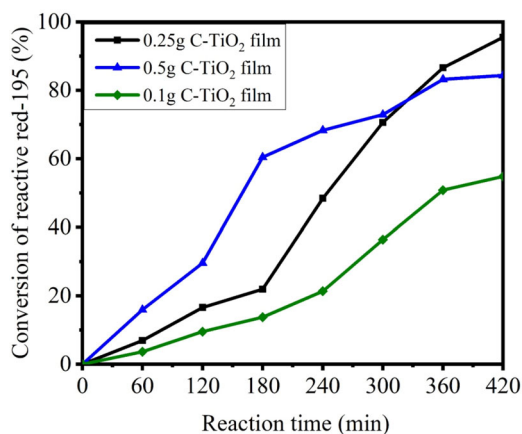


**Figure 11.** Conversion of RR-195 as a function of catalyst weights. Reaction conditions:  $[\text{RR-195}] = 0.02 \text{ g L}^{-1}$ ,  $V = 50 \text{ mL}$ ,  $\text{pH} = 6.26$ , ambient temperature.

compared to the bare CA sample and this could support this argument. The results suggest that the deposition of C-TiO<sub>2</sub> into CA enhanced the polymer chain durability, that could improve the mechanical and thermal stability of the film.

### Evaluation of catalytic activity

#### Effect of catalyst weight

Figure 11 illustrates the photocatalytic ability of catalytic mass for the decomposition RR-195 under visible light irradiation.

The experiment was conducted under normal conditions, the concentration of RR-195 was 20 ppm (a higher concentration than used by Habibi et al. who used nanocomposite cobalt catalyst coating on the Petri to decompose RR-195 with the concentration of 10 ppm (Habibi and Rezvani 2015), 50 mL RR-195 in a water solvent,  $\text{pH}$  of solution = 6.26. The results showed that after 420 min of irradiation, 0.25 g of C-TiO<sub>2</sub>/CA film had converted 95.3% of RR-195, higher than the case of using 0.50 g (84.38%) and 0.1 g C-TiO<sub>2</sub>/CA film (54.82%).

Considering these results, it could be clearly seen that when the catalyst weight range from 0.1 g to 0.25 g, RR-195 conversion drastically increased. Generally, the increase of catalyst leads to the increase of active sites and also the contact possibility for reactants with these sites on the surface of the materials. As a result, the photocatalytic conversion of the dye increased significantly.

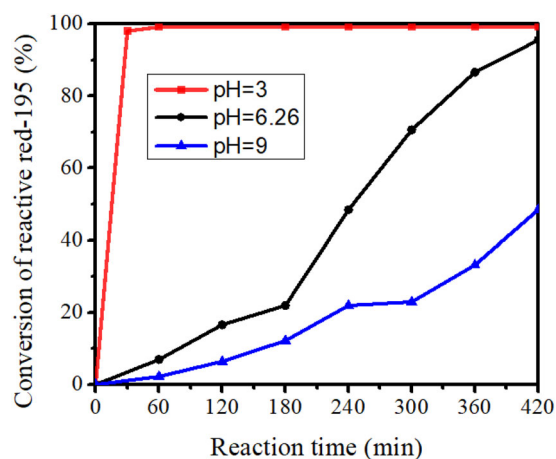


**Figure 12.** Conversion of RR-195 at different pH values. Reaction conditions:  $[\text{RR-195}] = 0.02 \text{ g L}^{-1}$ ,  $V = 50 \text{ mL}$ ,  $\text{pH} = 3, 6.26, \text{ and } 9$ ,  $m_{\text{catalyst}} = 0.25 \text{ g}$ , ambient temperature.

On the other hand, when the catalyst content exceeds the level of saturation, the proton absorption is reduced and this excess catalyst will create a secondary glow phenomenon, which reduces the contact area of the catalyst, thus lowering the photocatalytic activity. Additionally, it can be suggested that when the catalyst mass increases, the catalysts have the ability to shield each other, so that the catalyst in the back will not absorb the proton, which reduces the free radical. This phenomenon was also seen in other works (Papadam et al. 2007) (Lin et al. 2009; Rauf et al. 2011; Sleiman et al. 2007), which suggested that the agglomeration of TiO<sub>2</sub> significantly changed the efficiency in light absorption.

#### Effect of pH

$\text{pH}$  of the solution has a significant effect on the surface charge of TiO<sub>2</sub> because it could modify the adsorption capacity and then the photocatalytic process that takes place (Bourikas et al. 2005; Wang and Ku 2007). There is an isoelectric point (IEP) representing for  $\text{pH}$  at zero zeta voltage that can be used to evaluate the quality of the adsorbent surface. Experimentally, for TiO<sub>2</sub>, the isoelectric point ( $\text{pH}_{\text{iep}}$ ) is from 2 to 8.9 (Fernández-Ibáñez et al. 2003; Wang and Ku 2007). Nonetheless, the  $\text{pH}$  of P25 TiO<sub>2</sub> ranged from 6.2 to 6.9 (Bourikas et al. 2005; Dutta et al. 2004; Fernández-Ibáñez et al. 2003). In fact, the  $\text{pH}$  value of TiO<sub>2</sub> nanoparticles varies on the phase, the synthesis process, the material hydration, and the ion concentration in the solution

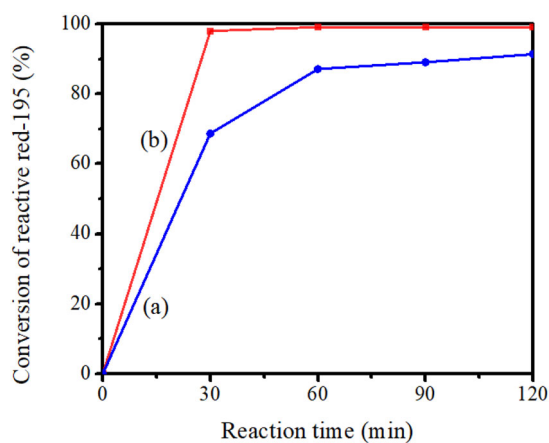
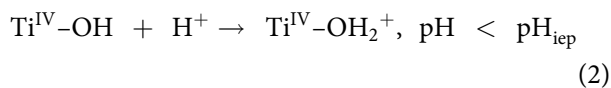


**Figure 13.** Conversion of RR-195 in the reaction using C-TiO<sub>2</sub> (a) and C-TiO<sub>2</sub>/CA (b) film as the catalyst. Reaction conditions: [RR-195] = 0.02 g L<sup>-1</sup>, V = 50 mL, pH = 3, ambient temperature.

(Allouni et al. 2009; Dutta et al. 2004; Fernández-Ibáñez et al. 2003; Pettibone et al. 2008).

Figure 12 shows the conversion of RR-195 at different pHs versus time. The results exhibited that at pH = 3 the ability to convert RR-195 on catalytic surfaces was optimal, reaching 99.15% after 60 min, higher than the results obtained at pH = 6.26 (95.53% after 420 min) and at pH = 9 (48.43% after 420 min). Theoretically, RR-195 reactive dye is anionic, so the conversion efficiency is higher at low pH because of the electrostatic attraction between anionic dye and positively-charged TiO<sub>2</sub> (pH < p*H*<sub>iep</sub>) following Equation (2) (Aguedach et al. 2005; Çiçek et al. 2007; Huang et al. 2008)



Beside pH which strongly influences the adsorption of the anionic dyes on the catalyst surface, the catalytic surface coverage also considerably affects the adsorption in the interface area between the catalytic surface and the dye. The anionic RR-195 accumulation in this area increases negative charges, which limits the adsorption of additional dye ions (Bhattacharyya et al. 2008). Moreover, when pH solution increase, the amount of negative charge on the catalyst surface upsurges that leads to the electrostatic repulsion (pH > p*H*<sub>iep</sub>). This phenomenon could drastically decrease the absorption of dye ions following Equation (3)

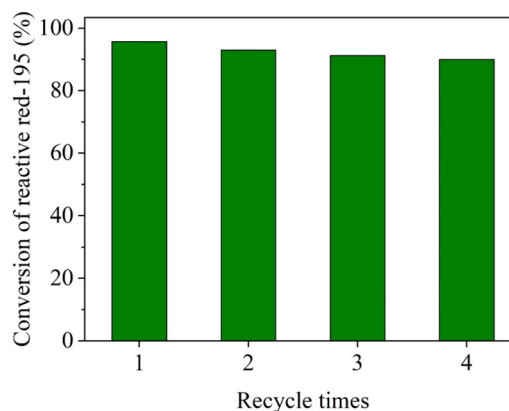
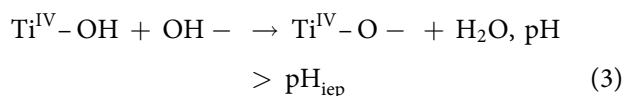


**Figure 14.** RR-195 conversion after four cycles of regeneration. Reaction conditions: 50 mL solution of RR-195 20 ppm, pH = 3, irradiation time = 60 min, ambient temperature.



This could derive from the particle size of the catalyst which toughly rely on the pH of the aqueous phase. Li et al. (2010) proposed that at neutral pH, the agglomeration of TiO<sub>2</sub> nanoparticles in aqueous phase happened. The change of pH to the acidic conditions could be a solution for this problem because TiO<sub>2</sub> nanoparticles size decreases at low pH. At this pH, the electrostatic repulsive forces between particles are minimized and the agglomeration will be limited.

To sum up, pH affects both the surface state of TiO<sub>2</sub> and the ionization of the dye as well as the particle size that affects the ability to transform RR-195. In this case, pH = 3 was the best condition for the degradation of RR-195 in the aqueous phase and this result is completely consistent with other studies (Aguedach et al. 2005; Bourikas et al. 2005).

#### Catalytic activity of C-TiO<sub>2</sub> and C-TiO<sub>2</sub>/AC film

The conversion of RR-195 in photocatalytic decomposition reaction using C-TiO<sub>2</sub> and C-TiO<sub>2</sub>/CA films as catalyst is exhibited in Figure 13.

It can be observed that the conversion using C-TiO<sub>2</sub>/CA was higher than using the C-TiO<sub>2</sub> catalyst after the same period of irradiation. Specifically, after 30 min of reaction, C-TiO<sub>2</sub>/CA catalyst for conversion efficiency RR-195 reached 98.02% while the C-TiO<sub>2</sub> catalyst reached only 68.71%. Then, after 60 min of reaction, with

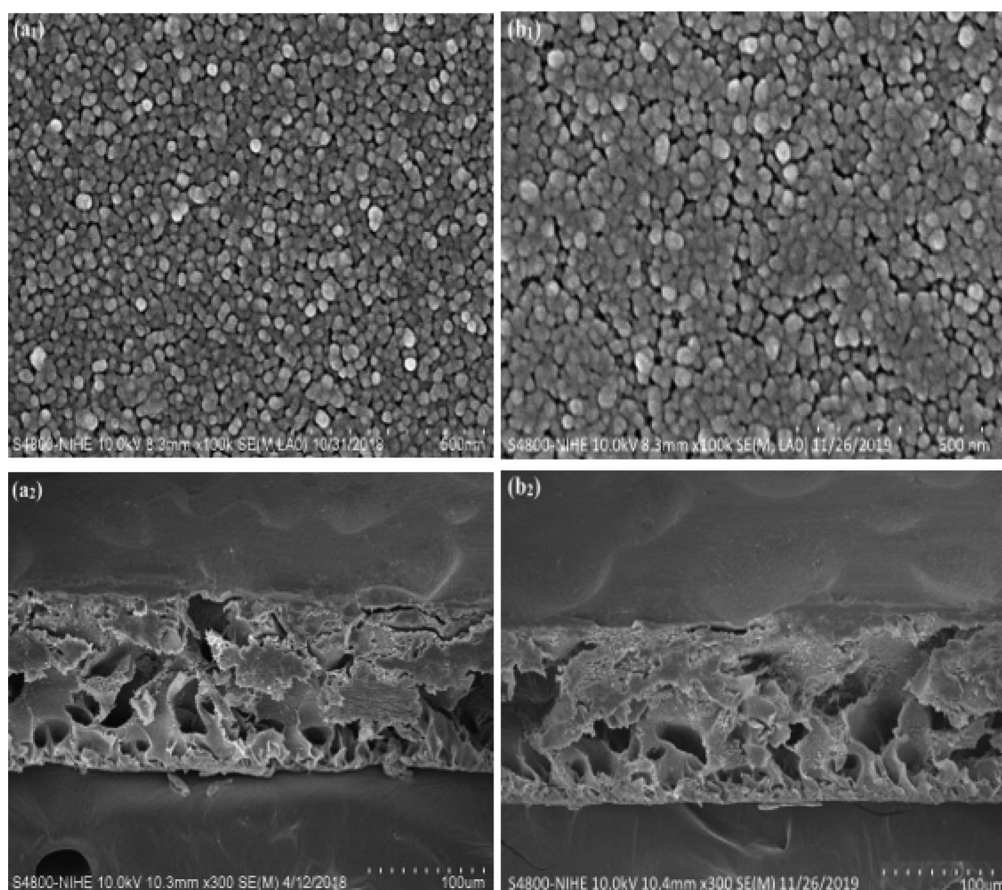


**Figure 15.** SEM images of the C-TiO<sub>2</sub>/CA films before (a<sub>1</sub>, a<sub>2</sub>) and after (b<sub>1</sub>, b<sub>2</sub>) reaction.

catalyst C-TiO<sub>2</sub>/CA the conversion efficiency for RR-195 reached 99.15% while the C-TiO<sub>2</sub> catalyst after 120 min only gave 91.43%. This could be explained by the C-TiO<sub>2</sub> dispersion on the CA film, which increases the area of light exposure and the adsorption capacity of RR-195 due to the porous system of the CA film (SEM images). Besides, in the case of using only C-TiO<sub>2</sub>, C-TiO<sub>2</sub> was evenly dispersed in the whole reaction device, so the exposure to light sources is usually concentrated only in some particles on the surface, the remaining particles situated at the reactor bottom could not absorb the light, reducing the possibility of ·OH radical generation, thus reducing the catalytic activity.

#### **Photocatalytic activity after recycling**

The ability to recover and reuse catalysts in photocatalysts plays a very important role as it contributes significantly to reducing operating costs in the wastewater treatment process. C-TiO<sub>2</sub> active sites are easily recovered after reaction due to its dispersion on the CA film. C-TiO<sub>2</sub>/CA

catalyst was regenerated by soaking, washing several times with distilled water and then dried naturally for use in evaluating catalytic reusability. The experiment was conducted at room temperature, pH = 3, 50 mL RR-195 20 ppm solution and irradiation time of 60 min. The conversion of the RR-195 using catalyst regenerated after four consecutive cycles is shown in Figure 14.

After four cycles of regeneration, the conversion efficiency of RR-195 still reached over 90%. Indeed, the conversion after the first cycle was 95.69% and after the 4th cycle was 90.02%. Performance has decreased slightly due to the deposition of intermediate products on the catalytic surfaces. For example, RR-195 contains sulfonate groups so sulfate ions certainly exist in the solution. These ions could bind strongly with the surface of the catalyst and deactivate some parts of the catalyst. As a result, the rate of oxidation reaction was diminished (Abdullah et al. 1990). A similar result was observed by Zhu et al. (2009) when they degraded Congo Red using chitosan/nano-CdS as the catalyst under visible light.

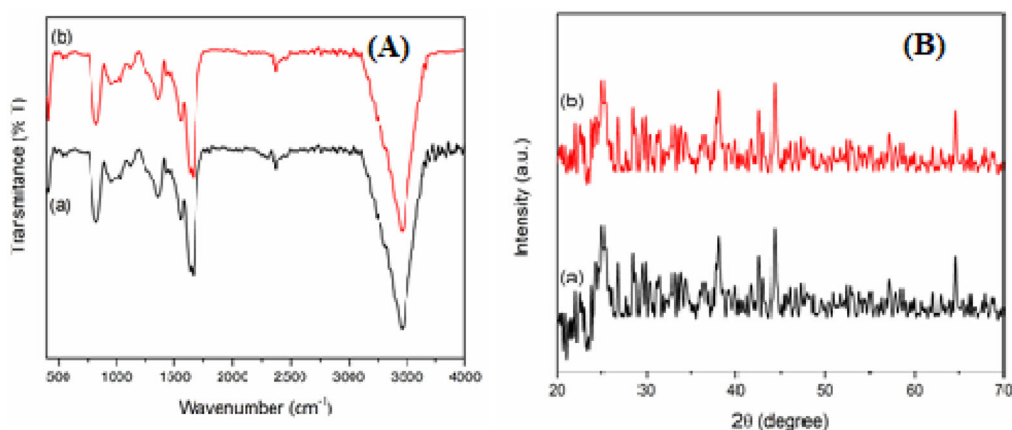


**Figure 16.** (A) FT-IR spectra and (B) XRD patterns of the C-TiO<sub>2</sub>/CA film before (a) and after (b) reaction.

However, the value of 90.02% is still impressive after several times of regeneration and completely readiness for reusability.

In addition, the photocatalyst film before and after the decomposition of RR-195 was analyzed by SEM images, FT-IR, and XRD. The SEM images of samples still kept the morphological structure of CA film and the size of C-TiO<sub>2</sub> was still at about 30 nm (Figure 15). It shows the FT-IR spectra of those two samples showed that the position of peaks were unchanged (Figure 16(A)). As shown in Figure 16(B), the XRD patterns of the samples in the range 2-theta of 20°–70°. According to XRD, the characteristic peaks of TiO<sub>2</sub> can be clearly observed, indicating its structure remains unchanged. The results suggest that the photocatalyst film is structure stable during the composition of RR-195.

The results revealed that the activity of the photocatalytic film changed negligibly, which indicates that the film is stable and effective for RR-195 decomposition and can be reused after up to four cycles.

## Conclusions

C-doped TiO<sub>2</sub> photocatalyst has been successfully synthesized from Binh Dinh ilmenite and *Stevia* leaves *via* the pyrolysis process. The experimental results proved that carbon had been successfully doped into the TiO<sub>2</sub> lattice by replacing oxygen atoms and creating oxygen vacancies, resulting in visible light absorption ability. The grafting of C-TiO<sub>2</sub> onto CA film improved the

photocatalytic activity of C-TiO<sub>2</sub> in the decomposition reaction of reactive dyes RR-195. The results also revealed that at low pH values there was a significant electrostatic interaction of positively charged catalytic surfaces and anionic dyes. The highest value of conversion achieved at pH = 3 was 99.15% after 60 min of visible light irradiation. Moreover, catalytic activity remained high after four cycles of regeneration. Therefore, high photocatalytic activity composite films can be considered promising material for organic pollutants treatment.

## Funding

This research was supported under the National Foundation for Science and Technology Development of Vietnam [Grant number 105.99-2018.301].

## ORCID

Huan V. Doan  <http://orcid.org/0000-0002-8757-364X>

## References

- Abdullah M, Low GKC, Matthews RW. 1990. Effects of common inorganic anions on rates of photocatalytic oxidation of organic carbon over illuminated titanium dioxide. *J Phys Chem.* 94(17):6820–6825. doi:10.1021/j100380a051
- Abedini R, Mousavi SM, Aminzadeh R. 2011. A novel cellulose acetate (CA) membrane using TiO<sub>2</sub> nanoparticles: preparation, characterization and permeation study. *Desalination.* 277(1–3):40–45. doi:10.1016/j.desal.2011.03.089
- Aguedach A, Brosillon S, Morvan J, Lhadi EK. 2005. Photocatalytic degradation of azo-dyes reactive black 5 and reactive yellow 145 in water over a newly deposited

- titanium dioxide. *Appl Catal B Environ.* 57(1):55–62. doi:10.1016/j.apcatb.2004.10.009
- Allouni ZE, Cimpan MR, Høl PJ, Skodvin T, Gjerdet NR. 2009. Agglomeration and sedimentation of TiO<sub>2</sub> nanoparticles in cell culture medium. *Colloid Surf B Biointerfaces.* 68(1):83–87. doi:10.1016/j.colsurfb.2008.09.014
- Bai H, Liu Z, Sun DD. 2010. Hierarchically multifunctional TiO<sub>2</sub> nano-thorn membrane for water purification. *Chem Commun.* 46(35):6542–6544. doi:10.1039/c0cc01143f
- Barndök H, Peláez M, Han C, Platten WE, Campo P, Hermosilla D, Blanco A, Dionysiou DD. 2013. Photocatalytic degradation of contaminants of concern with composite NF–TiO<sub>2</sub> films under visible and solar light. *Environ Sci Pollut Res.* 20(6):3582–3591. doi:10.1007/s11356-013-1550-z
- Bhattacharyya K, Varma S, Tripathi AK, Bharadwaj SR, Tyagi AK. 2008. Effect of vanadia doping and its oxidation state on the photocatalytic activity of TiO<sub>2</sub> for gas-phase oxidation of ethene. *J Phys Chem C.* 112(48):19102–19112. doi:10.1021/jp807860y
- Bourikas K, Styliidi M, Kondarides DI, Verykios XE. 2005. Adsorption of Acid Orange 7 on the surface of titanium dioxide. *Langmuir.* 21(20):9222–9230. doi:10.1021/la051434g
- Çiçek F, Özer D, Özer A, Özer A. 2007. Low cost removal of reactive dyes using wheat bran. *J Hazard Mater.* 146(1–2):408–416. doi:10.1016/j.jhazmat.2006.12.037
- Dutta PK, Ray AK, Sharma VK, Millero FJ. 2004. Adsorption of arsenate and arsenite on titanium dioxide suspensions. *J Colloid Interface Sci.* 278(2):270–275. doi:10.1016/j.jcis.2004.06.015
- Ernö P, Philippe B, Martin B. 2009. Structure determination of organic compounds, tables of spectral data, Fourth, Revised and Enlarged Edition. Berlin Heidelberg: Springer-Verlag.
- Fernández-Ibáñez P, Blanco J, Malato S, De Las Nieves FJ. 2003. Application of the colloidal stability of TiO<sub>2</sub> particles for recovery and reuse in solar photocatalysis. *Water Res.* 37(13):3180–3188. doi:10.1016/S0043-1354(03)00157-X
- Gaya UI, Abdullah AH. 2008. Heterogeneous photocatalytic degradation of organic contaminants over titanium dioxide: a review of fundamentals, progress and problems. *J Photochem Photobiol C Photochem Rev.* 9(1):1–12. doi:10.1016/j.jphotochemrev.2007.12.003
- Gong X, Lu W, Liu Y, Li Z, Shuang S, Dong C, Choi MMF. 2015. Low temperature synthesis of phosphorous and nitrogen co-doped yellow fluorescent carbon dots for sensing and bioimaging. *J Mater Chem B.* 3(33):6813–6819. doi:10.1039/C5TB00575B
- Huang Y, Ho W, Lee S, Zhang L, Li G, Yu JC. 2008. Effect of carbon doping on the mesoporous structure of nanocrystalline titanium dioxide and its solar-light-driven photocatalytic degradation of NO<sub>x</sub>. *Langmuir.* 24(7):3510–3516. doi:10.1021/la703333z
- Ibhadon A, Fitzpatrick P. 2013. Heterogeneous photocatalysis: recent advances and applications. *Catalysts.* 3(1):189–218. doi:10.3390/catal3010189
- Ioniiă M, Criță LE, Voicu SI, Dinescu S, Miculescu F, Costache M, Iovu H. 2018. Synergistic effect of carbon nanotubes and graphene for high performance cellulose acetate membranes in biomedical applications. *Carbohydr Polym.* 183:50–61. doi:10.1016/j.carbpol.2017.10.095
- Jinlong L, Lijuan D, Shuaiqiang J, Guozhe S, Yulin Z, Yan Z, Boxin L, Zhiyong X. 2018. Synthesis and photocatalytic properties of visible light-responsive, three-dimensional, flower-like La–TiO<sub>2</sub>/g–C<sub>3</sub>N<sub>4</sub> heterojunction composites. *RSC Adv.* 8:29645–29653. doi:10.1039/C8RA06466K
- Kamisaka H, Adachi T, Yamashita K. 2005. Theoretical study of the structure and optical properties of carbon-doped rutile and anatase titanium oxides. *J Chem Phys.* 123(8):084704. doi:10.1063/1.2007630
- Kang GD, Cao YM. 2014. Application and modification of poly(vinylidene fluoride) (PVDF) membranes – a review. *J Memb Sci.* 463:145–165. doi:10.1016/j.memsci.2014.03.055
- Kono H, Numata Y, Nagai N, Erata T, Takai M. 1999. CPMAS <sup>13</sup>C NMR and X-ray studies of cellooligosaccharide acetates as a model for cellulose triacetate. *J Polym Sci A Polym Chem.* 37(22):4100–4107. doi:10.1002/(SICI)1099-0518(19991115)37:22<4100::AID-POLA8>3.0.CO;2-D
- Kubacka A, Fernández-García M, Colón G. 2012. Advanced nanoarchitectures for solar photocatalytic applications. *Chem Rev.* 112(3):1555–1614. doi:10.1021/cr100454n
- Li G, Lv L, Fan H, Ma J, Li Y, Wan Y, Zhao XS. 2010. Effect of the agglomeration of TiO<sub>2</sub> nanoparticles on their photocatalytic performance in the aqueous phase. *J Colloid Interface Sci.* 348(2):342–347. doi:10.1016/j.jcis.2010.04.045
- Lin Y, Ferronato C, Deng N, Wu F, Chovelon J. M. 2009. Photocatalytic degradation of methylparaben by TiO<sub>2</sub>: multivariable experimental design and mechanism. *Appl Catal B Environ.* 88(1–2):32–41. doi:10.1016/j.apcatb.2008.09.026
- Liu F, Abed MRM, Li K. 2011. Preparation and characterization of poly(vinylidene fluoride) (PVDF) based ultrafiltration membranes using nano γ-Al<sub>2</sub>O<sub>3</sub>. *J Memb Sci.* 366(1–2):97–103. doi:10.1016/j.memsci.2010.09.044
- Liu F, Hashim NA, Liu Y, Abed MRM, Li K. 2011. Progress in the production and modification of PVDF membranes. *J Memb Sci.* 375(1–2):1–27. doi:10.1016/j.memsci.2011.03.014
- Habibi MH, Rezvani Z. 2015. Photocatalytic degradation of an azo textile dye (C.I. Reactive Red 195 (3BF)) in aqueous solution over copper cobaltite nanocomposite coated on glass by Doctor Blade method. *Spectrochim Acta Part A: Mol Biomol Spectrosc.* 147:173–177. doi:10.1016/j.saa.2015.03.077
- Meng F, Chae SR, Drews A, Kraume M, Shin HS, Yang F. 2009. Recent advances in membrane bioreactors (MBRs): membrane fouling and membrane material. *Water Res.* 43(6):1489–1512. doi:10.1016/j.watres.2008.12.044

- Momeni MM, Ahadzadeh I, Rahmati A. 2016a. Nitrogen, carbon and iron multiple-co doped titanium dioxide nanotubes as a new high-performance photo catalyst. *J Mater Sci: Mater Electron*. 27:8646–8653. doi:10.1007/s10854-016-4885-7
- Momeni MM, Mahvari M, Ghayeb Y. 2019. Photoelectrochemical properties of ironcobalt WTiO<sub>2</sub> nanotube photoanodes for water splitting and photocathodic protection of stainless steel. *J Electroanal Chem*. 832:7–23. doi:10.1016/j.jelechem.2018.10.035
- Momeni MM, Ghayeb Y, Mozafari AA. 2016b. Optical and photo catalytic characteristics of Ag<sub>2</sub>S/TiO<sub>2</sub> nanocomposite films prepared by electrochemical anodizing and SILAR approach. *J Mater Sci: Mater Electron*. 27: 11201–11210. doi:10.1007/s10854-016-5240-8
- Ortega-Liévana MC, Sánchez-López E, Hidalgo-Carrillo J, Marinas A, Marinas JM, Urbano FJ. 2012. A comparative study of photocatalytic degradation of 3-chloropyridine under UV and solar light by homogeneous (photo-Fenton) and heterogeneous (TiO<sub>2</sub>) photocatalysis. *Appl Catal B Environ*. 127:316–332. doi:10.1016/j.apcatb.2012.08.036
- Papadam T, Xekoukoulotakis NP, Poullos I, Mantzavinos D. 2007. Photocatalytic transformation of acid orange 20 and Cr(VI) in aqueous TiO<sub>2</sub> suspensions. *J Photochem Photobiol A Chem*. 186(2–3):308–315. doi:10.1016/j.jphotochem.2006.08.023
- Pelaez M, Nolan NT, Pillai SC, Seery MK, Falaras P, Kontos AG, Dunlop PSM, Hamilton JWJ, Byrne JA, O’Shea K, et al. 2012. A review on the visible light active titanium dioxide photocatalysts for environmental applications. *Appl Catal B Environ*. 125:331–349. doi:10.1016/j.apcatb.2012.05.036
- Pettibone JM, Cwiertny DM, Scherer M, Grassian VH. 2008. Adsorption of organic acids on TiO<sub>2</sub> nanoparticles: effects of pH, nanoparticle size, and nanoparticle aggregation. *Langmuir*. 24(13):6659–6667. doi:10.1021/la7039916
- Wang R, Hashimoto K, Fujishima A, Chikuni M, Kojima E, Kitamura A, Shimohigoshi M, Watanabe T. 1997. New preparation method of visible light responsive titanium dioxide photocatalytic films. *Nature*. 388(6641):431–432.
- Radha KS, Shobana KH, Tarun M, Mohan D. 2014. Studies on sulfonated styrene acrylonitrile and cellulose acetate blend ultrafiltration membranes. *Desalin Water Treat*. 52(1–3):459–469. doi:10.1080/19443994.2013.808486
- Rauf MA, Meetani MA, Hisaindee S. 2011. An overview on the photocatalytic degradation of azo dyes in the presence of TiO<sub>2</sub> doped with selective transition metals. *Desalination*. 276(1–3):13–27. doi:10.1016/j.desal.2011.03.071
- Sakthivel S, Kisch H. 2003. Daylight photocatalysis by carbon-modified titanium dioxide. *Angew Chem Int Ed*. 42(40):4908–4911. doi:10.1002/anie.200351577
- Shuaiqiang J, Jinlong L, Guozhe S, Lijuan D, Yulin Z, Yan Z, Boxin L. 2019. Synthesis of 3D flower-like structured Gd/TiO<sub>2</sub>@rGO nanocomposites via a hydrothermal method with enhanced visible-light photocatalytic activity. *RSC Adv*. 9:31177–31185. doi:10.1039/C9RA06045F
- Sleiman M, Vildoza D, Ferronato C, Chovelon J. M. 2007. Photocatalytic degradation of azo dye Metanil Yellow: optimization and kinetic modeling using a chemometric approach. *Appl Catal B Environ*. 77(1–2):1–11. doi:10.1016/j.apcatb.2007.06.015
- Su Y, Yu J, Lin J. 2007. Vapor-thermal preparation of highly crystallized TiO<sub>2</sub> powder and its photocatalytic activity. *J Solid State Chem*. 180(7):2080–2087. doi:10.1016/j.jssc.2007.04.028
- Sun X, Brückner C, Lei Y. 2015. One-pot and ultrafast synthesis of nitrogen and phosphorus co-doped carbon dots possessing bright dual wavelength fluorescence emission. *Nanoscale*. 7(41):17278–17282. doi:10.1039/C5NR05549K
- Wang C, Sun D, Zhuo K, Zhang H, Wang J. 2014. Simple and green synthesis of nitrogen-, sulfur-, and phosphorus-co-doped carbon dots with tunable luminescence properties and sensing application. *RSC Adv*. 4(96): 54060–54065. doi:10.1039/C4RA10885J
- Wang H, Quan X, Yu H, Chen S. 2008. Fabrication of a TiO<sub>2</sub>/carbon nanowall heterojunction and its photocatalytic ability. *Carbon NY*. 46(8):1126–1132. doi:10.1016/j.carbon.2008.04.016
- Wang L, Hall W. K. 1984. In situ laser Raman spectroscopy. *J Phys Chem*. 88:5831. doi:10.1021/j150668a018
- Wang SD, Ma Q, Liu H, Wang K, Ling LZ, Zhang KQ. 2015. Robust electrospinning cellulose acetate@TiO<sub>2</sub> ultrafine fibers for dyeing water treatment by photocatalytic reactions. *RSC Adv*. 5(51):40521–40530. doi:10.1039/C5RA03797B
- Wang WY, Ku Y. 2007. Effect of solution pH on the adsorption and photocatalytic reaction behaviors of dyes using TiO<sub>2</sub> and nafion-coated TiO<sub>2</sub>. *Colloid Surf A Physicochem Eng Asp*. 302(1–3):261–268. doi:10.1016/j.colsurfa.2007.02.037
- Zhang W, Zhu Y, Liu X, Wang D, Li J, Jiang L, Jin J. 2014. Salt-induced fabrication of superhydrophilic and underwater superoleophobic PAA-g-PVDF membranes for effective separation of oil-in-water emulsions. *Angew Chem Int Ed*. 53(3):856–860. doi:10.1002/anie.201308183
- Zhu H, Jiang R, Xiao L, Chang Y, Guan Y, Li X, Zeng G. 2009. Photocatalytic decolorization and degradation of Congo Red on innovative crosslinked chitosan/nano-CdS composite catalyst under visible light irradiation. *J Hazard Mater*. 169(1–3):933–940. doi:10.1016/j.jhazmat.2009.04.037